

Plasma volume considerations for analysis of gaseous and aerosol samples using laser-induced breakdown spectroscopy

J. E. Carranza and D. W. Hahn*

Department of Mechanical and Aerospace Engineering, University of Florida, Gainesville, Florida 32611-6300, USA. E-mail: dwhahn@ufl.edu

Received 25th June 2002, Accepted 25th September 2002

First published as an Advance Article on the web 9th October 2002

Three distinct characteristic plasma volumes were experimentally measured and are discussed in the context of the analysis of gaseous and aerosol systems using laser-induced breakdown spectroscopy. The resulting statistical sample volume, emission-based plasma volume, and the physical plasma volume, range between 1.2×10^{-3} and 2.4×10^{-3} cm³, and the variations are interpreted in terms of the intrinsic behavior of laser-induced plasma-particle interactions. Due to plasma non-homogeneity, the particle vaporization necessary for subsequent detection is limited to a plasma region somewhat smaller than the region defined by the physical plasma volume based on optical absorption. In contrast, the emission-based plasma volume, the largest of the three recorded volumes, reflects analyte emission following particle vaporization and diffusion, and is considered in terms of an equivalent emitting plasma volume.

Introduction

Laser-induced breakdown spectroscopy (LIBS), also known as laser-induced plasma spectroscopy, has been widely studied and implemented for the analysis of gaseous systems, including aerosol sample streams.^{1,2} LIBS has been successfully applied as an analytical technique for the determination of overall mass concentrations of aerosols and for the continuous on-line monitoring of effluent waste streams and aerosol loadings.³⁻⁷ In a series of recent studies Hahn and co-workers addressed the feasibility and applicability of LIBS for the detection and quantitative size analysis of individual aerosol particles.⁹⁻¹¹ Single-shot conditional analysis of LIBS spectra takes advantage of the discrete nature of aerosol particles and the point sampling volume realized with LIBS to collect and analyze individual aerosol particles and to improve the sensitivity of the LIBS technique. This methodology leads to an analysis approach that is rooted in a probabilistic model of collecting single aerosol particles in consideration of a characteristic plasma volume or plasma size. The size, characteristics, and physical meaning of the sampling plasma (*i.e.* plasma sample volume) are the focus of the current paper.

A more detailed explanation of the analysis of single aerosol particles using LIBS can be found in the above-cited references,⁸⁻¹¹ and only a short clarification of the dependence of the LIBS sample volume is given here. When an aerosol particle is engulfed (*i.e.* sampled) by a given laser-induced plasma, the event may be defined as a particle hit. The overall hit rate realized with single particle analysis may be modeled using a Poisson sampling probability, in which the probability of collecting at least a single particle in a given plasma volume is expressed as $F = 1 - \exp(-\mu)$, where F is the sampling frequency (*i.e.* particle hit rate), and μ is the average number of particles per plasma volume. The latter parameter is defined as $\mu = NV$, where N is the aerosol number density (number of particles/volume) and V is the plasma sample volume. It is noted that the sampling frequency may be approximated as $F \approx \mu \approx NV$ for small values of μ based on the small argument expansion of $e^{-\mu}$. Substituting the last relation into the probability function,

the following expression may be obtained for what is defined as the statistical plasma sample volume V_s

$$V_s = -\ln(1-F)/N. \quad (1)$$

The statistical sample volume is interpreted as the effective plasma sampling volume corresponding to a given particle sampling frequency of F realized at an aerosol number density N , where F is defined as the number of particle hits divided by the total number of laser shots for a given aerosol dispersion. To improve the analyte signal-to-noise ratio for low aerosol loadings, the actual aerosol mass concentration C (total aerosol analyte mass per volume of gas) can be determined using LIBS-based conditional data analysis as described previously.⁸ With this approach,

$$C = XF \quad (2)$$

where X is the equivalent aerosol mass concentration that is obtained by processing the ensemble-averaged LIBS spectrum corresponding to the aerosol particle hits only, and F is the aerosol sampling rate as described above. Note that as the sample rate approaches 100%, the conditional analysis scheme converges to traditional ensemble averaging of all LIBS spectra. In addition to the above calculations, the actual aerosol mass concentration may be defined using traditional aerosol mechanics as $C = \bar{m}N$, where \bar{m} is the mean aerosol analyte mass. Equating this last relation with eqn. 2, and making the small μ approximation ($F \approx NV$), yields the following

$$\bar{m}N = XNV \quad (3)$$

Eqn. 3 can be solved to yield the important LIBS relation $X = \bar{m}/V_e$, which defines what will be referred to in this paper as the emission-based sample volume V_e . This relation states that the LIBS-based analyte concentration of a single spectrum (based on the analyte atomic emission and a traditional calibration curve) corresponding to a single aerosol is related to the actual analyte mass contained in a characteristic (*i.e.*, emission-based) plasma volume. In other words, the emission-based sample volume can be defined as the required plasma

volume to yield an atomic emission-based mass concentration corresponding to the actual analyte mass of an individually sampled aerosol particle.

In this paper, both the statistical sample volume and the emission-based sample volume are evaluated along with a measured physical plasma volume based on plasma optical density. These three characteristic plasma volumes are discussed in concert to elucidate fundamental plasma-particle interactions, as well as to further the implementation of LIBS as an analytical technique suitable for the analysis of aerosol systems, notably individual aerosol particles.

Experimental system and methodology

Three complementary experiments were performed to assess the various laser-induced plasma volumes. In the first set of experiments, monodisperse silica particle aqueous suspensions were used to create aerosol streams with a known aerosol number density, enabling evaluation of the statistical sample volume. The second set of experiments was designed to calculate the LIBS-based equivalent mass concentration for various sized silica particles in order to evaluate the emission-based plasma volume. Finally, spatially and temporally resolved transmission measurements were recorded to provide a physical measure of the laser-induced plasma volume.

The LIBS experimental set-up and the aerosol generation system were presented in a previous paper,¹² and only a short description concerning the present study is given here. A 1064 nm Q-switched Nd:YAG laser operating with 315-mJ pulse energy, 10 ns pulse width, and 5 Hz pulse repetition rate, was used as the plasma source. An expanded laser beam 12 mm in diameter was focused using a 75 mm focal length UV grade plano-convex lens to an approximately 100- μm diameter spot to create the plasma inside the aerosol sample chamber. The plasma emission was collected along the incident beam in a backward direction and separated using a 50-mm diameter elliptical pierced mirror. The collected light was launched into an optical fiber bundle coupled to a spectrometer (2400 groove mm^{-1} grating, 0.12 nm optical resolution), and recorded with an intensified charge-coupled device (iCCD) array. Aerosols were generated by the nebulization of either aqueous solutions of silicon (ICP-grade silicon standards), or monodisperse silica particle suspensions. The nebulizer used 5 l min^{-1} (lpm) of dry nitrogen, and the nebulizer output was subsequently mixed with a gaseous co-flow stream of 42 lpm of purified, dry air. The nebulized aqueous silicon produced a high number density ($\sim 10^4 \text{ cm}^{-3}$) of submicron-sized silicon-rich particles through drying of the nebulized droplets in the purified air co-flow stream. Alternatively, spherical SiO_2 particles with monodisperse diameters ranging between 1.0, 1.5 and 2.1 μm were introduced into the co-flow stream through nebulization of particle suspensions. The concentration of the monodisperse silica particle suspensions was adjusted (using ultra-purified water dilution) prior to nebulization to produce aerosol particle number densities ranging from about 5 to 90 particles cm^{-3} in the LIBS sample chamber. As described in ref. 12, the aerosol system is designed such that the nebulizer exhausts directly into the center of a tapered mixing/drying section. The co-flow geometry shields the aerosols from the chamber walls, which are micropolished to prevent deposition. No independent measurements were performed to verify the aerosol number densities in the sample chamber.

All LIBS-based experiments used the neutral silicon atomic emission line at 288.16 nm. The processed LIBS signal was the ratio of the integrated atomic emission line peak area to the continuum base emission intensity, referred to as the peak-to-base (P/B) ratio. The continuum intensity was interpolated using the adjacent, featureless continuum emission intensity on both sides of the silicon emission line. For

temporal signal integration, the 288.16 nm Si I emission line intensity (peak-to-base) was optimized at 35 μs time delay with respect to the incident laser pulse, with an integration time of 5 μs . Ensemble averaging (minimum of 3000 individual spectra at each known aqueous silicon concentration) was used to construct a linear calibration response curve of the 288.16 nm silicon P/B signal as a function of known silicon mass concentration in the LIBS sample chamber. The calibration curve was highly linear ($R^2 > 0.99$) over the concentration range from 0 to 3030 $\mu\text{g m}^{-3}$, the highest concentration investigated.

Single-shot conditional analysis was used to identify and analyze individual spectra corresponding the various sized monodisperse silica particles. The conditional data analysis routine was reported previously,^{8,10} and involves the identification of individual LIBS spectra corresponding to the presence of discrete particles within a given plasma volume, based on the targeted analyte atomic emission signal exceeding a predetermined threshold value. The threshold is typically determined using an analyte free sample stream such that several false hits (*i.e.*, spectral noise) are obtained for a large a number of laser shots. For the current study, the threshold value for the 288.16-nm silicon emission peak was set to obtain an average of 15 false hits (*i.e.*, hits recorded for the nebulization of purified water) for every 1000 laser shots for nearly all experiments. False hits correspond to extreme spectral noise fluctuations arising from intensifier shot noise. To assess the effect of the threshold value, additional experiments were performed using a more restrictive threshold value such that about 2 false hits were recorded for each 1000 shots. For comparison, an average of 15.8 hits per 1000 shots with a standard deviation of 3.3 hits was recorded with purified water, and an average of 45.3 hits with a standard deviation of 4.7 was recorded for the silica particle-seeded aerosol stream. The difference yielded a silica particle sampling rate of 30.7 hits per 1000 shots with a standard deviation of 3.6 hits. Using the same experimental conditions but with the more restrictive sample threshold, experiments yielded an average of 1.8 hits per 1000 shots with a standard deviation of 0.42 recorded with purified water, and an average of 32.5 hits with a standard deviation of 3.6 recorded for the silica particle-seeded aerosol stream, for an overall sampling rate of 29.5 hits per 1000 shots with a standard deviation of 5.8. Comparison of the two sampling rates (30.7 ± 3.6 and 29.5 ± 5.8) reveals no statistical difference between the actual silica particle sample rates when using the two different conditional analysis threshold values. For all spectral data processing, individual spectra were smoothed using the Savitzky-Golay algorithm^{13,14} and subsequently processed using the P/B of the 288.16 nm silicon emission line profile.

To determine the exact number density of the silica microspheres in suspension prior to nebulization, transmission measurements were recorded for various dilutions of the prepared stock suspension. A 25 mW He:Ne laser operating at 632.8 nm was used to record the transmission through a standard 1 cm pathlength scattering cell. Transmission was recorded for various dilution factors with respect to the original silica particle suspension. The dilutions ranged from a factor of 3–6, and were selected to provide an optical density sufficiently small to ensure the absence of any multiple scattering effects.

For the physical plasma volume measurements, a probe Nd:YAG laser (532 nm, 6.4 ns pulse width) was synchronized to the plasma-creating laser. A time delay of zero between the two lasers was defined when the temporal peaks of both laser pulse profiles were coincident in time. The probe laser was then set to a time delay of 20 ns with respect to the plasma-creating laser, which placed the probe laser at the end of the plasma-creating laser pulse. Both the flashlamp and Q-switch of the probe laser were externally triggered using a digital delay

generator synchronized to the plasma-creating laser, resulting in less than 1 ns of jitter between the two pulses. The probe laser power was recorded with a volume-integrating laser pulse calorimeter (50 mm detector area), using a 1 min average at a 5 Hz repetition rate. The detector was placed about 1 m from the plasma to eliminate any detection of plasma emission. The large detector area negated any potential effects of beam steering on the recorded transmission, as the laser beam interacted with a small central fraction of the volume-integrating detector area, and no displacement was observed during the experiments. A two-axis precision stage was used to translate the 532-nm probe beam horizontally (x -coordinate) and vertically (y -coordinate) through the plasma at 90 degrees with respect to the plasma-creating laser pulse direction. A 200 mm plano-convex lens was mounted to the stage to focus the probe beam to a 200 μm spot within the laser-induced plasma volume. The probe laser beam was translated vertically through the plasma volume at each horizontal position, using 100 μm steps in the y -direction and 200- μm steps in the x -direction. The measurements were reported four times for each vertical traverse through the plasma.

Results and discussion

The determination of the statistical sample volume requires an accurate and independent calculation of the silica aerosol number density in the LIBS sample chamber. This is readily calculated from the gas co-flow rates and the rate at which liquid is nebulized, provided the number density of the silica particles in the liquid suspension is known. The suspension number density (N_{sus}) was determined from laser transmission measurements making use of the Beer–Lambert law

$$I/I_0 = \exp(-C_{\text{ext}} N_{\text{sus}} L) \quad (4)$$

where C_{ext} is the single particle extinction cross-section, and L is the optical path length (1 cm) through the scattering cell. Using complete Mie light scattering theory, an extinction cross-section of $8.80 \times 10^{-8} \text{ cm}^2$ was calculated for the 2.1 μm silica particles (refractive index = 1.46) in purified water (refractive index = 1.33). Using eqn. 4, the natural log of the transmission is linearly proportional to the extinction cross-section and the particle number density in suspension. As discussed above, the original suspension was diluted to ensure single-scattering, hence the number density in eqn. 4 may be modified as the original number density times a dilution factor f_d . A plot of the natural log of the transmission as a function of the product $C_{\text{ext}} f_d L$ is presented in Fig. 1, with the slope equal to the number density of the original silica particle suspension. The transmission measurements yielded a particle number density of $1.87 \times 10^7 \text{ cm}^{-3}$ for the stock 2.1 μm silica suspension. The highly linear relation ($R^2 = 0.9997$) observed in Fig. 1 suggests no multi-scattering effects and a high degree of precision in the measured particle concentration. It is noted that this value was in excellent agreement with the result obtained based on serial dilution of the initial suspension number density provided by the manufacturer. The particle concentration was subsequently scaled to reflect dilution for all additional experiments, enabling the generation of a range of known silica aerosol concentrations in the LIBS sample chamber. As is discussed above, the sample chamber was designed to minimize particle deposition within the chamber. Furthermore, the experimentally recorded silica particle hits rates were found to be very steady over periods up to 1 h, the longest time for which experiments were performed. The steady sample rates corroborate the nebulization rate of the silica microspheres based on the nebulizer output, in that a significant enrichment of silica in suspension due to preferential nebulization of water would result in a

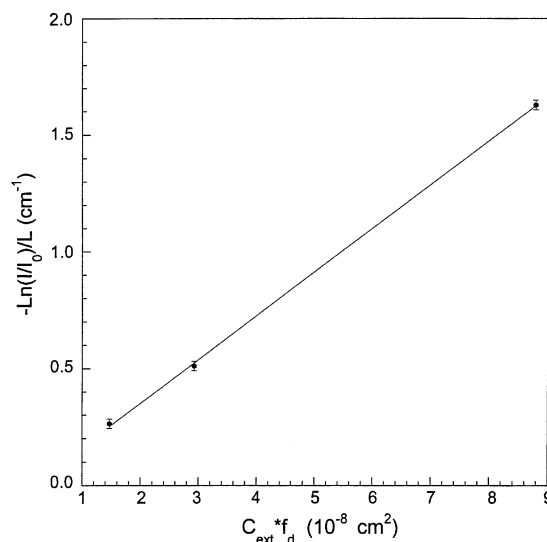


Fig. 1 The natural logarithm of the transmission as a function of the product of the extinction cross-section and dilution factor for the 2.1 μm silica particle suspensions. The error bars represent ± 1 standard deviation.

time-dependent silica particle suspension concentration and therefore a time-dependent silica particle hit rate.

For the determination of the statistical sample volume, the LIBS-based silica particle sampling hit rate was determined for various silica particle concentrations using the 2.1 μm silica particles. As noted above, the conditional analysis threshold value was set to allow the detection of about 15 false hits in 1000 shots. This was accomplished by setting the threshold in a purified air stream with the nebulization of only ultra-purified water. The actual hit rate was obtained by subtraction of the average number of false hits from the total number of hits recorded in a 1000-shot sequence for the nebulized silica particle suspensions. It is noted that for determination of the statistical sample rate, a particle hit corresponds to the presence of a silicon emission signal in excess of the threshold value, and does not indicate complete particle vaporization. The LIBS-based silica particle sampling rate, expressed as the $-\ln(1-F)$, is presented in Fig. 2 as a function of the predetermined silica particle number density in the LIBS sample chamber. A plot of the $-\ln(1-F)$ as a function of N is characterized by a slope equal to the statistical plasma sample volume

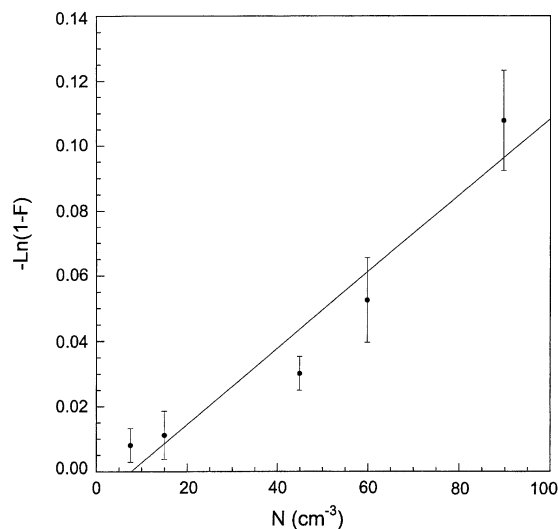


Fig. 2 The natural logarithm of one minus the experimental silica particle sampling rate as a function of the silica particle number density. The slope is equal to the statistical sample volume based on eqn. 1. The error bars represent ± 1 standard deviation.

V_s in consideration of Poisson sampling statistics and eqn. 1. A linear least squares fit ($R^2 = 0.931$) yielded a statistical plasma volume of $1.17 \times 10^{-3} \text{ cm}^3$, which corresponds to an equivalent spherical diameter of 1.3 mm. It is noted with regard to the Fig. 2 data that the observed sample frequency does not exactly follow an ideal Poisson probability distribution in that the observed rates tend to increase beyond those predicted at the upper and lower extremes. This deviation from the ideal linear trend could be due to aerosol–laser beam interactions before the laser focal region, an effect that may induce a particle breakdown sufficient to excite the analyte and trigger a conditional analysis hit. Such a breakdown would be decoupled from the actual laser-induced plasma volume, thereby inflating the sampling rate based on Poisson statistics as defined solely by the plasma volume.

To calculate the emission-based LIBS plasma volume, single-shot spectra corresponding to individual silica particles were collected and quantitatively analyzed for monodisperse silica particle diameters of 1.0, 1.5, and 2.1 μm . These particle sizes were all of a size characterized by complete particle vaporization, as determined in a recent study.¹⁷ It is known that single-shot LIBS spectra display considerable spectral noise as compared to ensemble-averaged spectra; hence it is desirable to improve the signal-to-noise ratio for quantitative analysis of spectra corresponding to the relatively small silica microspheres and hence relatively weak silicon emission line. Therefore, the Savitzky–Golay smoothing algorithm was used to suppress the level of random shot-noise for each spectrum identified as corresponding to a silica particle hit using the conditional analysis routine. This algorithm was found to have a negligible effect on the LIBS analyte signal (less than 1% change in the silicon emission line P/B ratio) as applied utilizing a filter template width greater than the line-width of the targeted atomic emission peak. After all single-shot spectra were smoothed, a spectral filtering algorithm was used to screen out false hits and other anomalous spectra (*e.g.*, particle breakdown outside of the plasma) resulting from the discrete sampling of the aerosol particles. The filtering algorithm was based on the similarity of the silicon emission line profile for a given single-shot spectrum as compared to the emission line profile corresponding to the ensemble-average of thousands of individual spectra recorded for the aqueous silicon standard solutions, as discussed above, on the same spectra used to generate the silicon LIBS calibration curve. This filtering algorithm resulted in the rejection of approximately 60% of all identified particle “hits,” consistent for all silica microsphere particle sizes, for the trigger threshold corresponding to an average of 15 false hits per 1000 shots. Using the spectral data processing schemes outlined above, all single-shot spectra were processed and a final ensemble-averaged spectrum was calculated for each silica particle size comprised of the individual single-shot spectra accepted after all data filtering. The P/B of the 288.16 nm silicon line was then calculated for each final ensemble-averaged spectrum, which was used with the silicon calibration curve to calculate the equivalent mass concentration X ($\mu\text{g m}^{-3}$) corresponding to each silica particle size. Fig. 3 presents the measured equivalent mass concentration as a function of the actual silicon mass contained in each single silica particle for the particle diameters of 1.0, 1.5, and 2.1 μm . The actual silicon mass is calculated based on a silica (SiO_2) particle density of 1.96 g cm^{-3} and a silicon (Si) mass fraction of 0.467. The highly linear behavior ($R^2 = 0.996$) observed in Fig. 3 enables a direct calculation of the emission-based plasma volume using the measured slope and the relation $X = \bar{m}/V_e$. This procedure yields a value of $2.38 \times 10^{-3} \text{ cm}^3$ with a corresponding equivalent spherical diameter of 1.66 mm.

The final experiment provided a physical measurement of the plasma volume induced by the 1064 nm Nd:YAG laser pulse. As described above, the plasma was formed in ambient air and probed using a 532 nm Nd:YAG pulse laser to determine the

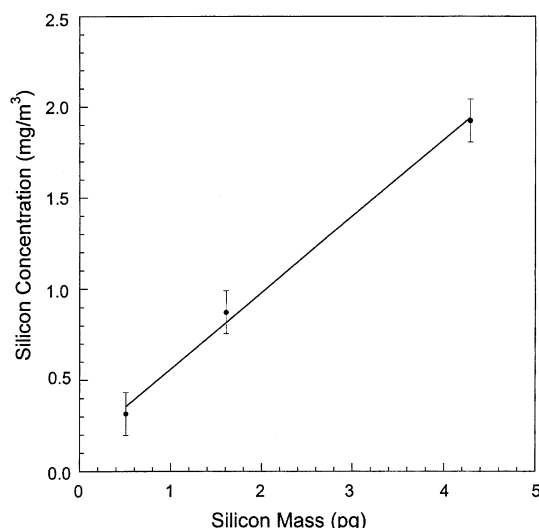


Fig. 3 The LIBS-based equivalent mass concentration of the 1.0, 1.5, and 2.1 μm silica particles as a function of the actual silicon mass contained in the silica particles. The error bars represent ± 1 standard deviation.

boundaries of the plasma at a 20 ns delay with respect to the 1064 nm plasma-initiating pulse. For a given point within the plasma, the transmission of the probe laser was calculated as the ratio of the probe pulse power through the laser-induced plasma to the probe laser power in the absence of the laser-induced plasma. As discussed above, it was determined that the laser-induced plasma emission contributed a negligible signal to the probe pulse power meter. The plasma boundary was defined as the point at which an optical thickness of 0.1 was recorded. The optical thickness is ideally defined as the weighted sum of the product of each absorbing species cross-section, absorbing species number density, and optical pathlength. No measurements of the absorption spectrum in the region near 532 nm were recorded; hence, the contribution of the measured absorption due to atoms (*e.g.* photoionization) or free electrons (free-free) is unknown. As such, the apparent plasma volume may be influenced by the choice of probe laser wavelength. The optical thickness is readily calculated as the opposite sign of the natural log of the transmission, as defined by the Beer–Lambert law. An optical thickness of 0.1 corresponds to the plasma absorbing approximately 10% of the probe laser energy. The plot of measured optical thickness *versus* distance for each traverse was used to define the plasma boundary by interpolating the resulting profile using a third order polynomial to define the exact point corresponding to an optical thickness of 0.1. A plot of the plasma volume cross-sectional profile is shown in Fig. 4. Also included in the figure is an ideal elliptical profile based on the measured plasma volume and plasma aspect ratio. A high degree of symmetry is observed in the Fig. 4 data, with the overall shape corresponding well to a prolate spheroid. This type of shape has been reported before for laser-induced plasmas^{15,16} and it is characteristic for high-energy pulses. A numerical integration of the measured profile yielded a physical plasma volume of $1.44 \times 10^{-3} \text{ cm}^3$, with an equivalent spherical diameter of 1.4 mm.

In this study, three different characteristic plasma volumes were determined using three different physical measurement schemes. The resulting plasma volumes have been defined as a statistical sample volume, an emission-based volume, and a physical plasma volume. The experimental results are summarized in Table 1, and while it is noted that all three plasma volumes agree to within a factor of 2, the actual differences should be interpreted in the context of the relevant plasma processes. To understand the relations between these different characteristic plasma volumes, it is useful to consider the

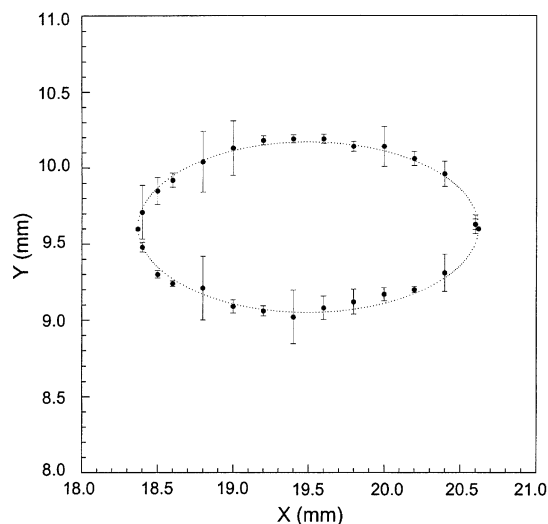


Fig. 4 Cross-section of the physical plasma profile measured at the end of the 1064 nm plasma-generating laser pulse. The boundary represents an optical thickness of 0.1 at 532 nm, and the error bars represent ± 1 standard deviation of the measured optical density. The dotted line is an elliptical profile fit to the experimental plasma volume and aspect ratio.

Table 1 Summary of the measured plasma volumes for a 315 mJ laser pulse energy. The plasma diameter reflects an equivalent spherical volume

Characteristic plasma	Volume/mm ³	Diameter/mm
Statistical	1.17	1.3
Physical	1.44	1.4
Emission-based	2.38	1.7

interaction of a single aerosol particle with the plasma as defined by the measured optical thickness of 0.1. The plasma itself must have a significant boundary region due to its highly transient nature and its formation within a continuum gaseous medium. With this in mind, the physical plasma volume is somewhat arbitrary, in that a larger plasma volume could be defined if experimental precision was sufficient to measure an optical thickness less than 0.1. However, while the physical plasma volume is defined in the current study based on optical thickness, it is recognized that as the plasma state weakens (e.g. reduction in temperature and free electron density) on the outer boundaries, energy may not be available to sufficiently vaporize a given aerosol particle in this regime. With the additional need for particle vaporization with LIBS-based aerosol analysis, consideration of the physical plasma volume gives way to the statistical plasma volume. The statistical sampling volume ($V_s = F/N$) represents the effective volume consistent with the LIBS system to detect the presence of an individual particle following sufficient vaporization and subsequent analyte species atomic emission.

There was no *a priori* basis in the present study to expect complete convergence of the physical and statistical plasma volumes. Nonetheless, the current data suggest that sufficient vaporization for subsequent analyte detection is confined within a region somewhat smaller than the region defined by an optical thickness of 0.1. For the current study, defining the physical plasma volume to a region based on an optical thickness of 0.15 (at 532 nm) yields convergence between the physical and statistical sample volumes. The important conclusion is not the degree of exactitude between these two characteristic plasma volumes, but rather that the plasma volume is not ideally homogeneous with regard to plasma-particle interactions. Additional plasma transmission measurements, including Abel inversion and plasma modeling, may provide

further insight into the local plasma state conditions necessary for particle sampling and quantitative analysis.

In contrast to particle sampling considerations, once the particle is vaporized and ionized, a different set of processes are relevant to LIBS-based analysis. It is expected that the analyte mass released from the aerosol particle will subsequently diffuse throughout the plasma volume with a relatively short time-scale. Hence, it follows that the analyte atomic emission and plasma continuum emission that are collected and reported as the signal peak-to-base ratio reflect a plasma volume characteristic of the entire emitting plasma at the relevant signal integration delay time, typically microseconds to tens of microseconds following plasma initiation. The emission-based plasma volume reflects this LIBS signal corresponding to the particle analyte mass contained in an equivalent emitting plasma volume. Using the expressions derived above, this relation may be expressed as the analyte P/B yielding the LIBS-based equivalent mass concentration, which is equal to the actual analyte mass divided by the emission-based plasma volume V_e . In view of the present data (see Table 1), it is reasonable to conclude that the emitting plasma volume extends beyond the plasma size as defined by the limit necessary for initial particle vaporization (sampling volume) or an optical thickness of 0.1 (physical volume). Because the equivalent mass concentration is linearly proportional to the peak-to-base ratio (by the calibration curve), the calculated emission-based plasma volume (*i.e.* emitting volume) is independent of the size of the particle, provided complete particle vaporization exists, as demonstrated by the linear response observed in Fig. 3.

In summary, the analysis of individual aerosol particles using laser-induced plasma spectroscopy has been discussed in the context of the characteristic plasma volumes. While the statistical sample volume reflects the probabilistic nature of capturing single particles using the laser-induced plasma, the statistical volume also reflects a fundamental threshold necessary for significant vaporization of the sampled particle. In contrast, both the physical and emission-based plasma volumes are characterized by the absorption or emission properties of the plasma state, respectively, with the latter coupled to the additional considerations of plasma-induced particle vaporization and analyte diffusion. While all three characteristic plasma volumes were found to be of similar value in the present study, each is coupled to specific plasma processes, and when considered together they provide additional insight into the plasma processes relevant to LIBS-based aerosol analysis.

References

- 1 D. A. Rusak, B. C. Castle, B. W. Smith and J. D. Winefordner, *Crit. Rev. Anal. Chem.*, 1997, **27**, 257–290.
- 2 K. Song, Y.-I. Lee and J. Sneddon, *Appl. Spectrosc. Rev.*, 1997, **32**, 183–235.
- 3 L. J. Radziemski, T. R. Loree, D. A. Cremers and N. M. Hoffman, *Anal. Chem.*, 1983, **55**, 1246–1252.
- 4 R. E. Neuhauser, U. Panne, R. Niessner, G. A. Petrucci, P. Cavalli and N. Omenetto, *Anal. Chim. Acta*, 1997, **346**, 37–48.
- 5 J. P. Singh, F. Y. Yueh, H. S. Zhang and R. L. Cook, *Process Control Qual.*, 1997, **10**, 247–258.
- 6 N. E. Neuhauser, U. Panne, R. Niessner and P. Wilbring, *Fresenius' J. Anal. Chem.*, 1999, **364**, 720–726.
- 7 H. Zhang, F. Y. Yueh and J. P. Singh, *Appl. Opt.*, 1999, **38**, 1459–1466.
- 8 D. W. Hahn, W. L. Flower and K. R. Hencken, *Appl. Spectrosc.*, 1997, **51**, 1836–1844.
- 9 D. W. Hahn, *Appl. Phys. Lett.*, 1998, **72**, 2960–2962.
- 10 D. W. Hahn and M. M. Lunden, *Aerosol Sci. Technol.*, 2000, **33**, 30–48.
- 11 J. E. Carranza, B. T. Fisher, G. D. Yoder and D. W. Hahn, *Spectrochim. Acta, Part B*, 2001, **56**, 851–864.
- 12 D. W. Hahn, J. E. Carranza, G. R. Arsenault, H. A. Johnsen and K. R. Hencken, *Rev. Sci. Instrum.*, 2001, **72**, 3706–3713.

- 13 A. Savitzky and M. J. E. Golay, *Anal. Chem.*, 1964, **36**, 1627–1639.
- 14 H. H. Madden, *Anal. Chem.*, 1978, **50**, 1383–1386.
- 15 A. Borghese and S. S. Merola, *Appl. Opt.*, 1998, **37**, 3977–3983.
- 16 Y. L. Chen, J. W. L. Lewis and C. Parigger, *J. Quant. Spectrosc. Radiat. Transfer*, 2000, **67**, 91–103.
- 17 J. E. Carranza and D. W. Hahn, *Anal. Chem.*, 2002, in the press.